Journal of Hydraulic Research

ISSN: (Print) (Online) Journal homepage: https://www.tandfonline.com/loi/tjhr20

Experiments on two-layer stratified gravity currents in the slumping phase

Ching-Sen Wu & Albert Dai

To cite this article: Ching-Sen Wu & Albert Dai (2020) Experiments on two-layer stratified gravity currents in the slumping phase, Journal of Hydraulic Research, 58:5, 831-844, DOI: 10.1080/00221686.2019.1671517

To link to this article: https://doi.org/10.1080/00221686.2019.1671517

IAHR AIRH
Taylor & Francis
Taylor & Francis Group

Journal of Hydraulic Research Vol. 58, No. 5 (2020), pp. 831–844
https://doi.org/10.1080/00221686.2019.1671517

Research paper

Experiments on two-layer stratified gravity currents in the slumping phase

CHING-SEN WU, Assistant Professor, *Department of Civil Engineering, National Ilan University, Yilan, Taiwan*
Email: olivercswu@niu.edu.tw

ALBERT DAI, Professor, *Department of Engineering Science and Ocean Engineering, National Taiwan University, Taipei, Taiwan*
Email: hdai@ntu.edu.tw (author for correspondence)

ABSTRACT
Experiments on gravity currents produced from full-depth two-layer stratified buoyancy sources propagating in the slumping phase are presented in the paper. The Froude number in the slumping phase, $\mathsf{F_S} = U_f/\sqrt{g_0' H}$, where U_f is the front velocity, g_0' is the average reduced gravity and H is the lock height, is influenced by the density difference ratio, $\mathsf{R_R} = (\rho_U - \rho_0)/(\rho_L - \rho_0)$, and the buoyancy distribution parameter, $\mathsf{R_B} = B_U/(B_L + B_U)$, where ρ_U, ρ_L and ρ_0 are the fluid densities in the upper layer, lower layer and ambient environment while B_U and B_L represent the buoyancies in the upper layer and lower layer. The flow morphology of two-layer stratified gravity currents in the slumping phase can be categorized into two different regimes, demarcated by $\mathsf{R_B} \approx 0.6$. For $\mathsf{R_B} < 0.6$, the gravity currents are dominated by the lower layer and the lower layer takes the lead throughout the slumping phase. The Froude number in the slumping phase for $\mathsf{R_B} < 0.6$ increases as $\mathsf{R_R}$ decreases from unity. For $\mathsf{R_B} > 0.6$, the gravity currents are dominated by the upper layer and the upper layer overrides and outruns the lower layer. The Froude number in the slumping phase for $\mathsf{R_B} > 0.6$ decreases as $\mathsf{R_R}$ decreases from unity. As $\mathsf{R_B} \approx 0.6$, the upper layer and lower layer propagate forward approximately at the same speed and the Froude number in the slumping phase maintains at $\mathsf{F_S} \approx 0.46$ irrespective of the density difference ratio. For weakly stratified two-layer buoyancy source, $\mathsf{R_R} \to 1$, the influence of the buoyancy distribution parameter diminishes and the Froude number in the slumping phase approaches $\mathsf{F_S} \approx 0.45$.

Keywords: Buoyancy-driven flows; convection; stratified flows and density currents

1 Introduction

Gravity currents, also known as density currents, occur when a denser fluid propagates into a lighter one primarily in a horizontal direction. The density differences can be caused by variations in salinity, temperature and concentration of suspended particles in natural and man-made environments. Examples of gravity currents include sea breezes, dust storms, snow avalanches and pyroclastic flows, which are ubiquitous in our environment. A detailed account of the diversity of gravity currents and their relevances is given by Simpson (1997).

The interests in gravity currents have initiated a series of theoretical, experimental and computational studies since the 1950s. To date, most works focus on such flows in a confined channel, namely the lock-exchange experiment, over a horizontal boundary (Adduce, Sciortino, & Proietti, 2012; La Rocca, Adduce, Lombardi, Sciortino, & Hinkelmann, 2012; La Rocca, Adduce, Sciortino, & Pinzon, 2008; La Rocca, Adduce, Sciortino, Pinzon, & Boniforti, 2012; Marino, Thomas, & Linden, 2005; Nogueira, Adduce, Alves, & Franca, 2013a, 2013b, 2014; Shin, Dalziel, & Linden, 2004), on a favourable slope (Dai, 2013a, 2013b, 2014) and on an adverse slope (Jones, Cenedese, Chassignet, Linden, & Sutherland, 2014; Lombardi, Adduce, Sciortino, & La Rocca, 2015; Marleau, Flynn, & Sutherland, 2014; Ottolenghi, Adduce, Inghilesi, Roman, & Armenio, 2016). In this experimental set-up, fluids of different densities are initially filled in different parts of the channel separated by a barrier. The two fluids are then set into motion when the barrier is removed. The heavy fluid travels along the bottom of the channel in the streamwise direction underneath the ambient fluid, while the ambient light fluid moves along the upper surface in the opposite direction. The propagation of gravity currents produced in lock-exchange experiments can be categorized into three different phases of spreading in sequence, namely the slumping, inertial and viscous phases. After the heavy fluid is released from the lock, the gravity currents accelerate from rest and then propagate at a constant speed in the slumping phase. Afterwards, depending on the Reynolds number, the gravity currents may go through the inertial and viscous phases or directly to the viscous phase

Received 9 October 2018; accepted 16 September 2019/Open for discussion until 31 March 2021.

ISSN 0022-1686 print/ISSN 1814-2079 online
http://www.tandfonline.com

(Cantero, Lee, Balachandar, & Garcia, 2007; Huppert, 1982). For two-layer flows, as demonstrated by Ungarish (2009), the propagation is first dominated by the inertial-buoyancy balance, then transition to the viscous-buoyancy balance phase occurs. In-depth discussions of the history of lock-exchange experiments can be found in the literature (e.g. Borden & Meiburg, 2013; Shin et al., 2004; Ungarish, 2009; Ungarish & Hogg, 2018) and references given therein.

While most works focus on the gravity currents produced from a homogeneous buoyancy source, less is known about those produced from stratified buoyancy sources. In fact, stratification in the vertical direction, due to processes such as variations in settling velocity of particles, turbulence intensity and entrainment of ambient fluid, is commonly seen in nature. The stratification is known to have a significant influence on the propagation of gravity currents and we attempt to address this issue of stratified gravity currents in the slumping phase following our previous work of stratified gravity currents in the inertial phase (Dai, 2017). In the literature, a number of investigations focus on the propagation of gravity currents into density stratified environments, e.g. bottom-propagating gravity currents (Birman, Meiburg, & Ungarish, 2007; Khodkar, Nasr-Azadani, & Meiburg, 2018; Maxworthy, Leilich, Simpson, & Meiburg, 2002; Tan, Nobes, Fleck, & Flynn, 2010; Ungarish, 2006; Ungarish & Huppert, 2002, 2004, 2006; White & Helfrich, 2008, 2012) and intrusive gravity currents (Amen & Maxworthy, 1980; Bolster, Hang, & Linden, 2008; Cheong, Kuenen, & Linden, 2006; Flynn & Linden, 2006; Flynn & Sutherland, 2004; Johnson et al., 2015; Khodkar, Allam, & Meiburg, 2018; Khodkar, Nasr-Azadani, & Meiburg, 2016; Schooley & Hughes, 1972; Ungarish, 2005; Wu, 1969). Gravity currents produced from two-layer stratified buoyancy sources and propagating in the inertial phase were investigated experimentally by Gladstone, Ritchie, Sparks, and Woods (2004) followed by Dai (2017). In conjunction with the scaling analysis, it has been reported by Dai (2017) that the flow morphology depends on the two dimensionless parameters, namely the density difference ratio between the upper layer and lower layer :

$$\mathsf{R_R} = \frac{\rho_U - \rho_0}{\rho_L - \rho_0}, \tag{1}$$

where ρ_U, ρ_L and ρ_0 represent the fluid densities in the upper layer, lower layer and ambient environment, respectively, and the buoyancy distribution parameter:

$$\mathsf{R_B} = \frac{B_U}{B_U + B_L} \tag{2}$$

where $B_U = g(\rho_U - \rho_0)h_U L_0/\rho_0$ and $B_L = g(\rho_L - \rho_0)h_L L_0/\rho_0$ represent the buoyancy in the upper layer and that in the lower layer, respectively, and h_U, h_L and L_0 represent the initial thickness of the upper layer, initial thickness of the lower layer and the lock length of the heavy fluid. When $\mathsf{R_R} \to 1$, the buoyancy source is termed "weakly stratified" as compared with $\mathsf{R_R} \ll 1$, which is termed "strongly stratified". The distinction of a "weakly" stratified source and a "strongly" stratified one is made at the authors' discretion in order to highlight different flow morphologies. When $\mathsf{R_B} \to 1$, the gravity currents are dominated by the upper layer, while $\mathsf{R_B} \ll 1$, the gravity currents are dominated by the lower layer. Therefore, it is anticipated that at an intermediate, critical value of $\mathsf{R_B}$, i.e. when $B_L \approx B_U$, the upper layer and lower layer can propagate forward at the same speed and we will show that, based on the experiments, this critical value is $\mathsf{R_B} \approx 0.6$.

This study is a continuation of the scaling analysis and the experiments for the gravity currents produced from two-layer stratified sources propagating in the inertial phase (Dai, 2017). In this study, we investigate the same problem, i.e. gravity currents produced from two-layer density stratified sources, but, rather than on the inertial phase of motion, our focus is on the slumping phase during which the front velocity keeps approximately constant in the propagation. For the readers' convenience, here we follow Dai (2017) and use the same dimensionless parameters, i.e. $\mathsf{R_R}$ and $\mathsf{R_B}$, to characterize the two-layer stratified buoyancy source. The Froude number in the slumping phase is defined as:

$$\mathsf{F_S} = \frac{U_f}{\sqrt{g_0' H}} \tag{3}$$

where U_f is the front speed, g_0' is the average reduced gravity and H is the lock height. The average reduced gravity is defined in terms of the average density of two-layer source, ρ_C, and the density of homogeneous ambient fluid, ρ_0, as:

$$g_0' = \frac{\rho_C - \rho_0}{\rho_0} g \tag{4}$$

where $\rho_C = \rho_L h_L/H + \rho_U h_U/H$. Here the density difference is sufficiently small and the gravity currents can be classified as Boussinesq.

For the gravity currents which are produced from a full-depth homogeneous buoyancy source propagating in the slumping phase, Benjamin's energy-conserving theory (Benjamin, 1968) predicts that $\mathsf{F_S} = 0.5$. Keulegan's and Barr's experiments (Barr, 1967; Keulegan, 1958) showed that there is a slight increase in $\mathsf{F_S}$ with Reynolds number; however, the increase in $\mathsf{F_S}$ becomes less pronounced for Reynolds numbers greater than 1000. For full-depth lock-exchange experiments with a rigid top surface, it was reported that $\mathsf{F_S} \approx 0.46$ for Reynolds numbers greater than 1000. Additionally, the Froude number based on shallow-water prediction (Ungarish, 2009) and theoretical derivation (Hogg, Nasr-Azadani, Ungarish, & Meiburg, 2016), namely $\mathsf{F_S} = 0.47$, are also close to the reported values. We should remark that the classic case of gravity currents produced from a full-depth homogeneous buoyancy source serves as a benchmark and is equivalent to $\mathsf{R_B} \to 0$ or $\mathsf{R_B} \to 1$, and $\mathsf{R_R} \to 1$ in our framework.

In the literature, a number of studies have been focused on quantifying the entrainment coefficients through the volume-based entrainment method or measuring the ratio of mixing layer thicknesses (e.g. Dimotakis, 2000; Ellison & Turner, 1959; Koochesfahani & Dimotakis, 1986; Samasiri & Woods, 2015). More recent investigation on quantifying the mixing dynamics uses the particle image velocimetry and planar laser induced fluorescence measurement technique simultaneously (Balasubramanian & Zhong, 2018). In this study, our objective is to deepen the understanding of gravity currents produced from two-layer stratified sources propagating in the slumping phase by identifying how the two dimensionless parameters, R_R and R_B, influence the Froude number in the slumping phase and the flow morphology through qualitative observations based on our experiments. The paper is organized as follows. In Section 2, the experimental set-up and procedures for the stratified gravity currents in the slumping phase are described. In Section 3, the results on selected cases to illustrate different flow morphologies and Froude number in the slumping phase are presented. Conclusions are made in Section 4.

2 Experimental set-up

A sketch of the lock-exchange experiment for the two-layer stratified gravity currents is shown in Fig. 1. The experiments were conducted in a transparent Perspex channel with a rectangular cross-section, 0.2 m wide, 0.3 m deep and 2.4 m long. The channel is divided into two parts by a removable gate, placed at a distance $L_0 = 0.964$ m away from the left wall. The left region is filled with two layers of heavy fluid, of which the excess density is created using sodium chloride. The right region is filled with homogeneous ambient fluid, i.e. freshwater. Both the two-layer heavy fluid on the left and the homogeneous ambient fluid on the right of the gate are filled to the same height, $H = 0.2$ m. The lower layer thickness and the upper layer thickness were varied in the ranges of $0.050 \le h_L/H \le 1.000$ and $0.240 \le h_U/H \le 0.950$ while $h_L + h_U = H$ was maintained throughout the experiments. Two sheets of Perspex were in contact with the top fluid boundary and the two sheets were separated by a thin gap to allow easy withdrawal of the gate.

We used an LED light board and a light-diffusing screen against the back wall of the channel to provide uniform illumination. A Canon 700D (Tokyo, Japan) camera was positioned 10 m away from the front wall of the channel and operated with a resolution of 1920 × 1080 pixel at 24 frames per second. The recorded images were exported to a PC for postprocessing. For flow visualization, blue and yellow colours were chosen for the lower and upper layers, respectively and the ambient fluid, shown as white in the images, was not coloured. The lower layer was coloured with 2.5 ml of blue dye per 1.0 l of heavy fluid and the upper layer was coloured with 4.5 ml of yellow dye per 1.0 l of heavy fluid. The experimental set-up in this study is similar to the set-up given in Dai (2017), to which the readers are referred for more details.

Fluid densities were measured using a density meter with an accuracy of 10^{-4} g cm^{-3}. Compared with the excess density created by sodium chloride, the density variations due to temperature changes are relatively small to affect the results. The fluid density of ambient environment was $\rho_0 = 0.9960 \pm 0.0012$ g cm^{-3} and the average density of the two-layer fluid was carefully maintained at $\rho_C = 1.0400$ g cm^{-3}. The kinematic viscosity of both the heavy and ambient light fluids is taken as $\nu = 1.1 \times 10^{-2}$ cm^2 s^{-1}. The Reynolds number in the experiments, defined as $\mathsf{R}_\mathsf{e} = UH/\nu$, where $U = \sqrt{g_0' H}$ is the velocity scale and H is the length scale, was approximately $\mathsf{R}_\mathsf{e} \approx 53{,}000$. The Reynolds number in all experiments was far in excess of 1000, above which the viscous effects are thought to be unimportant (Simpson, 1997).

3 Results

A series of 49 experiments were conducted for the two-layer stratified gravity currents in the slumping phase. The operational parameters and measured experimental results are listed in Tables 1 and 2. In each experimental set-up, five repeated runs were performed to make qualitative and quantitative observations. The density difference ratio covers a range of

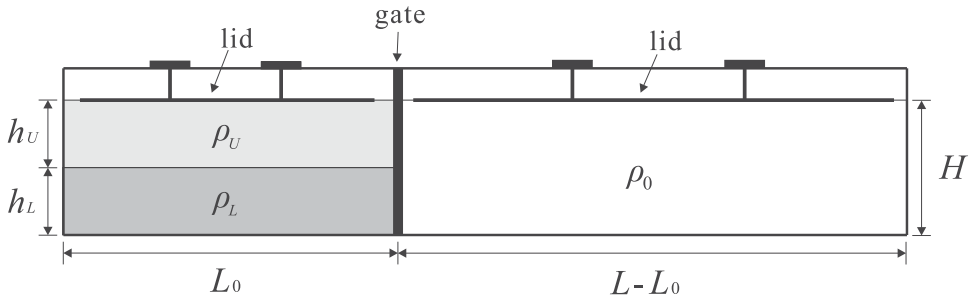

Figure 1 Sketch of the lock-exchange experiment for gravity currents produced from two-layer stratified buoyancy sources. The left region is filled with two layers of heavy fluid, where ρ_L and ρ_U represent the fluid densities in the lower layer and upper layer and h_L and h_U represent the thicknesses in the lower layer and upper layer, respectively. The ambient fluid has density ρ_0. The depth of fluid is maintained at $H = 20$ cm. The total length of the channel is $L = 240$ cm while the lock gate is placed at a distance $L_0 = 96.4$ cm from the left wall. The top fluid boundary is in contact with a rigid lid

Table 1 Operational parameters for the gravity currents produced from a full-depth two-layer stratified buoyancy source in the slumping phase, including the thicknesses of the lower and upper layers normalized by the total fluid depth, i.e. h_L/H and h_U/H, the average density of heavy fluid ρ_C, fluid densities in the lower layer and in the upper layer, i.e. ρ_L and ρ_U, and the density of ambient fluid ρ_0

Experiment	h_L/H	h_U/H	ρ_C (g cm^{-3})	ρ_L (g cm^{-3})	ρ_U (g cm^{-3})	ρ_0 (g cm^{-3})
A1	1.000	–	1.0400	1.0400	–	$0.9960^{+0.0001}_{-0.0000}$
B1	0.445	0.555	1.0400	1.0758	1.0113	$0.9953^{+0.0001}_{-0.0000}$
B2	0.545	0.455	1.0400	1.0607	1.0151	$0.9955^{+0.0001}_{-0.0000}$
B3	0.615	0.385	1.0400	1.0532	1.0189	$0.9960^{+0.0000}_{-0.0001}$
B4	0.665	0.335	1.0400	1.0489	1.0222	$0.9953^{+0.0001}_{-0.0001}$
B5	0.705	0.295	1.0400	1.0458	1.0260	$0.9953^{+0.0000}_{-0.0000}$
B6	0.735	0.265	1.0400	1.0438	1.0293	$0.9954^{+0.0001}_{-0.0002}$
B7	0.760	0.240	1.0400	1.0422	1.0328	$0.9956^{+0.0001}_{-0.0001}$
C1	0.320	0.680	1.0400	1.0916	1.0159	$0.9970^{+0.0001}_{-0.0000}$
C2	0.410	0.590	1.0400	1.0709	1.0184	$0.9960^{+0.0002}_{-0.0003}$
C3	0.485	0.515	1.0400	1.0598	1.0215	$0.9960^{+0.0000}_{-0.0001}$
C4	0.540	0.460	1.0400	1.0534	1.0243	$0.9960^{+0.0002}_{-0.0003}$
C5	0.585	0.415	1.0400	1.0487	1.0278	$0.9954^{+0.0002}_{-0.0001}$
C6	0.620	0.380	1.0400	1.0457	1.0308	$0.9962^{+0.0001}_{-0.0002}$
C7	0.650	0.350	1.0400	1.0432	1.0340	$0.9969^{+0.0001}_{-0.0001}$
D1	0.230	0.770	1.0400	1.1117	1.0185	$0.9955^{+0.0001}_{-0.0001}$
D2	0.310	0.690	1.0400	1.0814	1.0214	$0.9956^{+0.0001}_{-0.0000}$
D3	0.375	0.625	1.0400	1.0666	1.0241	$0.9956^{+0.0002}_{-0.0001}$
D4	0.430	0.570	1.0400	1.0578	1.0266	$0.9955^{+0.0002}_{-0.0001}$
D5	0.475	0.525	1.0400	1.0519	1.0293	$0.9956^{+0.0001}_{-0.0000}$
D6	0.510	0.490	1.0400	1.0476	1.0320	$0.9957^{+0.0002}_{-0.0001}$
D7	0.545	0.455	1.0400	1.0444	1.0347	$0.9956^{+0.0000}_{-0.0000}$
E1	0.165	0.835	1.0400	1.1292	1.0222	$0.9957^{+0.0003}_{-0.0001}$
E2	0.230	0.770	1.0400	1.0916	1.0245	$0.9956^{+0.0000}_{-0.0001}$
E3	0.285	0.715	1.0400	1.0731	1.0268	$0.9959^{+0.0001}_{-0.0000}$
E4	0.335	0.665	1.0400	1.0624	1.0288	$0.9953^{+0.0001}_{-0.0001}$
E5	0.375	0.625	1.0400	1.0545	1.0313	$0.9948^{+0.0000}_{-0.0001}$
E6	0.410	0.590	1.0400	1.0496	1.0333	$0.9954^{+0.0000}_{-0.0000}$
E7	0.445	0.555	1.0400	1.0456	1.0356	$0.9958^{+0.0001}_{-0.0002}$
F1	0.120	0.880	1.0400	1.1441	1.0257	$0.9963^{+0.0001}_{-0.0001}$
F2	0.165	0.835	1.0400	1.1013	1.0276	$0.9966^{+0.0001}_{-0.0002}$
F3	0.210	0.790	1.0400	1.0796	1.0294	$0.9960^{+0.0001}_{-0.0000}$
F4	0.250	0.750	1.0400	1.0662	1.0313	$0.9966^{+0.0002}_{-0.0002}$
F5	0.285	0.715	1.0400	1.0575	1.0329	$0.9964^{+0.0000}_{-0.0001}$
F6	0.320	0.680	1.0400	1.0510	1.0346	$0.9962^{+0.0000}_{-0.0002}$
F7	0.350	0.650	1.0400	1.0467	1.0365	$0.9965^{+0.0002}_{-0.0001}$
G1	0.080	0.920	1.0400	1.1604	1.0297	$0.9957^{+0.0003}_{-0.0002}$
G2	0.115	0.885	1.0400	1.1125	1.0307	$0.9957^{+0.0003}_{-0.0002}$

(*Continued*)

Table 1 Continued.

Experiment	h_L/H	h_U/H	ρ_C (g cm^{-3})	ρ_L (g cm^{-3})	ρ_U (g cm^{-3})	ρ_0 (g cm^{-3})
G3	0.145	0.855	1.0400	1.0864	1.0320	$0.9960^{+0.0000}_{-0.0002}$
G4	0.175	0.825	1.0400	1.0707	1.0334	$0.9964^{+0.0002}_{-0.0004}$
G5	0.205	0.795	1.0400	1.0603	1.0348	$0.9964^{+0.0001}_{-0.0002}$
G6	0.230	0.770	1.0400	1.0534	1.0360	$0.9958^{+0.0001}_{-0.0001}$
G7	0.255	0.745	1.0400	1.0475	1.0374	$0.9958^{+0.0001}_{-0.0001}$
H1	0.050	0.950	1.0400	1.1821	1.0329	$0.9956^{+0.0002}_{-0.0000}$
H2	0.070	0.930	1.0400	1.1229	1.0338	$0.9955^{+0.0001}_{-0.0000}$
H3	0.090	0.910	1.0400	1.0930	1.0347	$0.9960^{+0.0000}_{-0.0002}$
H4	0.110	0.890	1.0400	1.0756	1.0356	$0.9954^{+0.0001}_{-0.0000}$
H5	0.130	0.870	1.0400	1.0633	1.0365	$0.9960^{+0.0000}_{-0.0002}$
H6	0.150	0.850	1.0400	1.0550	1.0374	$0.9964^{+0.0000}_{-0.0000}$
H7	0.165	0.835	1.0400	1.0489	1.0382	$0.9957^{+0.0003}_{-0.0002}$

Note: The total fluid depth is $H = 20$ cm. The average density of the two-layer heavy fluid in the lock, $\rho_C = 1.0400$ g cm^{-3}, was maintained unchanged. At least five repeated runs were conducted for each experimental set-up.

Table 2 Experimental constants for the gravity currents produced from a full-depth two-layer stratified buoyancy source in the slumping phase, including the buoyancy distribution parameter $\mathsf{R_B}$, the density difference ratio $\mathsf{R_R}$, front velocity in the slumping phase U_f, the t-intercept in the plot of front position versus time, $L_C = U_f\,(t + t_0)$ and the Froude number in the slumping phase $\mathsf{F_S}$

Experiment	$\mathsf{R_B}$	$\mathsf{R_R}$	U_f (cm s^{-1})	$-t_0$ (s)	dδ/dt (cm s^{-1})	$\mathsf{F_S}$
A1	0.5	1.0	$13.20^{+0.14}_{-0.04}$	$0.09^{+0.02}_{-0.04}$	–	$0.450^{+0.002}_{-0.004}$
B1	0.2	0.2	$16.36^{+0.21}_{-0.14}$	$0.15^{+0.04}_{-0.03}$	0.83	$0.551^{+0.007}_{-0.005}$
B2	0.2	0.3	$15.43^{+0.05}_{-0.05}$	$0.14^{+0.10}_{-0.09}$	0.90	$0.522^{+0.002}_{-0.002}$
B3	0.2	0.4	$14.67^{+0.08}_{-0.09}$	$0.05^{+0.04}_{-0.04}$	1.05	$0.498^{+0.003}_{-0.003}$
B4	0.2	0.5	$14.50^{+0.06}_{-0.10}$	$0.08^{+0.02}_{-0.04}$	1.26	$0.489^{+0.002}_{-0.004}$
B5	0.2	0.6	$13.92^{+0.04}_{-0.09}$	$0.05^{+0.05}_{-0.04}$	1.43	$0.470^{+0.001}_{-0.003}$
B6	0.2	0.7	$13.89^{+0.12}_{-0.10}$	$0.09^{+0.06}_{-0.05}$	1.44	$0.469^{+0.004}_{-0.004}$
B7	0.2	0.8	$13.79^{+0.13}_{-0.07}$	$0.08^{+0.05}_{-0.07}$	1.44	$0.465^{+0.005}_{-0.002}$
C1	0.3	0.2	$15.85^{+0.15}_{-0.15}$	$0.08^{+0.10}_{-0.06}$	0.89	$0.545^{+0.005}_{-0.005}$
C2	0.3	0.3	$15.51^{+0.06}_{-0.08}$	$0.05^{+0.05}_{-0.03}$	0.94	$0.526^{+0.002}_{-0.003}$
C3	0.3	0.4	$14.93^{+0.05}_{-0.12}$	$0.03^{+0.02}_{-0.03}$	1.11	$0.506^{+0.002}_{-0.004}$
C4	0.3	0.5	$14.61^{+0.15}_{-0.07}$	$0.05^{+0.07}_{-0.03}$	1.33	$0.502^{+0.005}_{-0.003}$
C5	0.3	0.6	$13.99^{+0.16}_{-0.08}$	$0.05^{+0.07}_{-0.03}$	1.49	$0.478^{+0.006}_{-0.003}$
C6	0.3	0.7	$13.89^{+0.03}_{-0.05}$	$0.14^{+0.09}_{-0.09}$	1.51	$0.473^{+0.001}_{-0.002}$
C7	0.3	0.8	$13.45^{+0.11}_{-0.13}$	$0.07^{+0.06}_{-0.04}$	1.55	$0.462^{+0.004}_{-0.005}$
D1	0.4	0.2	$15.58^{+0.27}_{-0.12}$	$0.09^{+0.04}_{-0.07}$	0.90	$0.526^{+0.009}_{-0.004}$
D2	0.4	0.3	$15.47^{+0.07}_{-0.06}$	$0.04^{+0.05}_{-0.03}$	0.99	$0.523^{+0.003}_{-0.002}$
D3	0.4	0.4	$14.99^{+0.04}_{-0.07}$	$0.04^{+0.03}_{-0.02}$	1.98	$0.507^{+0.001}_{-0.002}$
D4	0.4	0.5	$14.69^{+0.06}_{-0.07}$	$0.05^{+0.04}_{-0.04}$	2.26	$0.496^{+0.002}_{-0.002}$
D5	0.4	0.6	$14.38^{+0.05}_{-0.05}$	$0.04^{+0.02}_{-0.01}$	2.41	$0.486^{+0.002}_{-0.002}$

(*Continued*)

Table 2 Continued.

Experiment	R_B	R_R	U_f (cm s^{-1})	$-t_0$ (s)	dδ/dt (cm s^{-1})	F_S
D6	0.4	0.7	$13.85^{+0.10}_{-0.17}$	$0.07^{+0.07}_{-0.07}$	2.57	$0.469^{+0.004}_{-0.006}$
D7	0.4	0.8	$13.70^{+0.12}_{-0.17}$	$0.05^{+0.02}_{-0.03}$	2.73	$0.463^{+0.004}_{-0.006}$
E1	0.5	0.2	$15.02^{+0.05}_{-0.07}$	$0.03^{+0.08}_{-0.03}$	0.89	$0.508^{+0.002}_{-0.002}$
E2	0.5	0.3	$14.96^{+0.13}_{-0.18}$	$0.08^{+0.09}_{-0.07}$	1.22	$0.506^{+0.004}_{-0.006}$
E3	0.5	0.4	$14.62^{+0.09}_{-0.12}$	$0.10^{+0.04}_{-0.06}$	1.94	$0.496^{+0.003}_{-0.004}$
E4	0.5	0.5	$14.53^{+0.13}_{-0.07}$	$0.09^{+0.12}_{-0.07}$	2.15	$0.490^{+0.004}_{-0.010}$
E5	0.5	0.6	$14.03^{+0.08}_{-0.13}$	$0.09^{+0.12}_{-0.09}$	2.55	$0.474^{+0.003}_{-0.004}$
E6	0.5	0.7	$13.96^{+0.02}_{-0.03}$	$0.07^{+0.03}_{-0.03}$	2.58	$0.471^{+0.001}_{-0.001}$
E7	0.5	0.8	$13.79^{+0.08}_{-0.04}$	$0.05^{+0.09}_{-0.04}$	2.77	$0.469^{+0.009}_{-0.003}$
F1	0.6	0.2	$13.35^{+0.10}_{-0.25}$	$0.11^{+0.03}_{-0.02}$	1.01	$0.455^{+0.004}_{-0.009}$
F2	0.6	0.3	$13.36^{+0.10}_{-0.09}$	$0.06^{+0.03}_{-0.04}$	1.77	$0.455^{+0.004}_{-0.003}$
F3	0.6	0.4	$13.63^{+0.17}_{-0.06}$	$0.06^{+0.01}_{-0.02}$	2.71	$0.463^{+0.006}_{-0.002}$
F4	0.6	0.5	$13.69^{+0.04}_{-0.05}$	$0.09^{+0.07}_{-0.06}$	2.79	$0.466^{+0.002}_{-0.002}$
F5	0.6	0.6	$13.63^{+0.04}_{-0.03}$	$0.09^{+0.08}_{-0.07}$	2.75	$0.467^{+0.008}_{-0.003}$
F6	0.6	0.7	$13.60^{+0.06}_{-0.16}$	$0.21^{+0.10}_{-0.08}$	3.08	$0.463^{+0.002}_{-0.006}$
F7	0.6	0.8	$13.60^{+0.14}_{-0.11}$	$0.34^{+0.05}_{-0.05}$	3.04	$0.463^{+0.004}_{-0.002}$
G1	0.7	0.2	$12.21^{+0.14}_{-0.18}$	$0.12^{+0.08}_{-0.04}$	–	$0.413^{+0.005}_{-0.006}$
G2	0.7	0.3	$12.55^{+0.10}_{-0.12}$	$0.48^{+0.10}_{-0.12}$	0.94	$0.425^{+0.004}_{-0.004}$
G3	0.7	0.4	$12.93^{+0.21}_{-0.12}$	$0.52^{+0.10}_{-0.10}$	1.21	$0.439^{+0.007}_{-0.004}$
G4	0.7	0.5	$13.16^{+0.10}_{-0.12}$	$0.24^{+0.08}_{-0.10}$	1.21	$0.449^{+0.003}_{-0.004}$
G5	0.7	0.6	$13.23^{+0.08}_{-0.11}$	$0.19^{+0.07}_{-0.11}$	1.23	$0.452^{+0.003}_{-0.004}$
G6	0.7	0.7	$13.37^{+0.15}_{-0.22}$	$0.18^{+0.11}_{-0.12}$	1.21	$0.453^{+0.005}_{-0.008}$
G7	0.7	0.8	$13.50^{+0.09}_{-0.08}$	$0.06^{+0.04}_{-0.04}$	1.21	$0.457^{+0.003}_{-0.003}$
H1	0.8	0.2	$12.51^{+0.14}_{-0.07}$	$0.10^{+0.10}_{-0.08}$	–	$0.423^{+0.005}_{-0.003}$
H2	0.8	0.3	$12.82^{+0.19}_{-0.15}$	$0.08^{+0.09}_{-0.06}$	–	$0.433^{+0.007}_{-0.005}$
H3	0.8	0.4	$12.96^{+0.24}_{-0.12}$	$0.26^{+0.13}_{-0.11}$	–	$0.440^{+0.008}_{-0.004}$
H4	0.8	0.5	$13.04^{+0.03}_{-0.04}$	$0.12^{+0.06}_{-0.05}$	1.22	$0.441^{+0.001}_{-0.001}$
H5	0.8	0.6	$13.06^{+0.01}_{-0.01}$	$0.06^{+0.04}_{-0.04}$	1.22	$0.443^{+0.001}_{-0.001}$
H6	0.8	0.7	$13.17^{+0.03}_{-0.06}$	$0.08^{+0.09}_{-0.07}$	1.25	$0.450^{+0.001}_{-0.002}$
H7	0.8	0.8	$13.30^{+0.17}_{-0.16}$	$0.13^{+0.03}_{-0.03}$	1.25	$0.450^{+0.006}_{-0.005}$

Note: The error estimates are to add and subtract the maximum and minimum values and should not be understood as the rms estimates.

$0.2 \leq R_R \leq 0.8$ and the buoyancy distribution parameter covers a range of $0.2 \leq R_B \leq 0.8$ in this study. As will be shown more clearly, the propagation of two-layer stratified gravity currents in the slumping phase can be categorized into two different regimes, demarcated by $R_B \approx 0.6$.

The cases presented in the paper are selected to highlight distinct flow morphologies and the influence of the two dimensionless parameters, i.e. R_R and R_B, on the Froude number in the slumping phase. First, the gravity currents in the slumping phase produced from a full-depth homogeneous buoyancy source, which serves as the limiting cases of $R_B \to 0$ or $R_B \to 1$, and $R_R \to 1$ in our framework, is revisited in Section 3.1. Second, the two-layer stratified gravity currents in the slumping phase, which can be categorized into those dominated by the lower layer and those dominated by the upper layer, are presented in Sections 3.2 and 3.3.

3.1 *Gravity currents produced from a homogeneous source*

Experiments on gravity currents produced from a full-depth homogeneous buoyancy source, listed in Tables 1 and 2 as *A*1, are reported in this section. The heavy fluid of density $\rho_C = 1.0400\,\mathrm{g\,cm^{-3}}$ and ambient light fluid of density $\rho_0 = 0.9960\,\mathrm{g\,cm^{-3}}$ were initially separated by a lock gate.

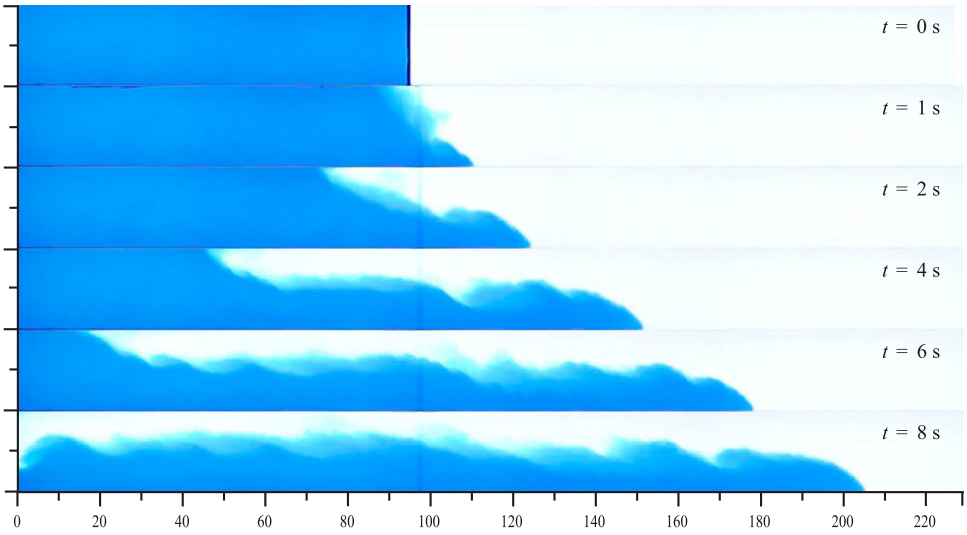

Figure 2 Experiment $06/16/16 - A1$: flow images for the gravity currents produced from a full-depth homogeneous buoyancy source. Distances in x and y directions are in units of cm. Time instances are chosen at $t = 0, 1, 2, 4, 6, 8$ s. The slumping phase begins at $t \approx 1.6$ s and the front velocity in the slumping phase is $U_f \approx 13.20\,\text{cm s}^{-1}$

Gravity currents were initiated when the lock gate was removed. Figure 2 shows the flow images at several time instances for the gravity currents produced from a homogeneous source. As the heavy fluid moves along the bottom and the ambient fluid moves along the top boundary in the opposite direction, Kelvin–Helmholtz billows, which are characteristic for gravity currents in the slumping phase (Cantero et al., 2007), form along the interface between the heavy and light fluids.

The front position, L_C, is measured from the lock gate to the leading edge of the gravity currents using the recorded images. Figure 3 shows the front position history of the gravity currents produced from a homogeneous buoyancy source. It is clear that the front position history approaches the straight line of best fit after $t \approx 1.6$ s and the departure from the best fit prior to $t \approx 1.6$ s represents that the gravity currents were accelerating from rest. The front velocity in the slumping phase is taken as the slope of the line of best fit and in experiment $06/16/16 - A1$ as shown in Fig. 3, $L_C = 13.20(t - 0.11)$ and $U_f \approx 13.20\,\text{cm s}^{-1}$. Based on our experiments, the Froude number in the slumping phase, defined by Eq. (3), is found to be $\mathsf{F_S} = 0.450^{+0.002}_{-0.004}$, which is consistent with reported values in the literature (Barr, 1967; Cantero et al., 2007; Hogg et al., 2016; Keulegan, 1958; Marino et al., 2005; Shin et al., 2004; Ungarish, 2009).

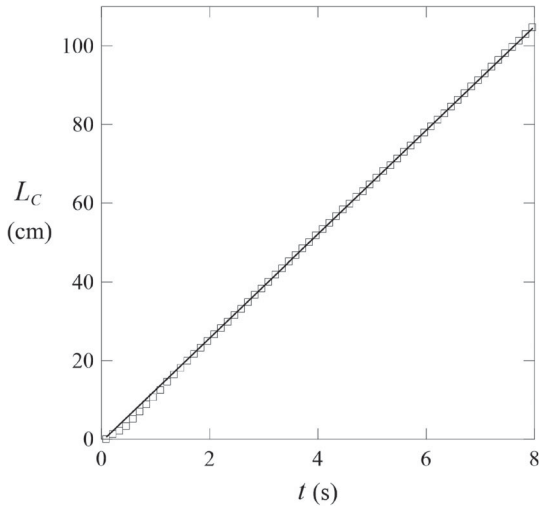

Figure 3 Experiment $06/16/16 - A1$: front position history for the gravity currents produced from a full-depth homogeneous buoyancy source. The solid line represents the straight line of best fit to the slumping phase of propagation and the fitting equation is $L_C = 13.20(t + t_0)$, where $t_0 = -0.11$ s is the t-intercept in the plot of L_C against time

3.2 *Stratified gravity currents dominated by the lower layer,* $0 < \mathsf{R_B} < 0.6$

In this section, we present the case when the stratified gravity currents are dominated by the lower layer, $0 < \mathsf{R_B} < 0.6$. It is observed that, in this flow regime, the lower layer takes the lead throughout the propagation of gravity currents in the slumping phase. The density difference ratio can influence the mixing between the two layers. In the experiments, the average density of the two-layer stratified heavy fluid and the density of ambient fluid remain unchanged. Such lower layer dominated gravity currents can be produced from a strongly stratified source, $\mathsf{R_R} \ll 1$, or from a weakly stratified source, $\mathsf{R_R} \to 1$, and we shall present these flows in order.

3.2.1 *Strongly stratified two-layer source,* $\mathsf{R_R} \ll 1$

For stratified gravity currents dominated by the lower layer and produced from a strongly stratified two-layer source, Fig. 4 shows the flow images of experiment $08/22/16 - B1$ at $\mathsf{R_B} = 0.2$ and $\mathsf{R_R} = 0.2$. After the two-layer stratified heavy

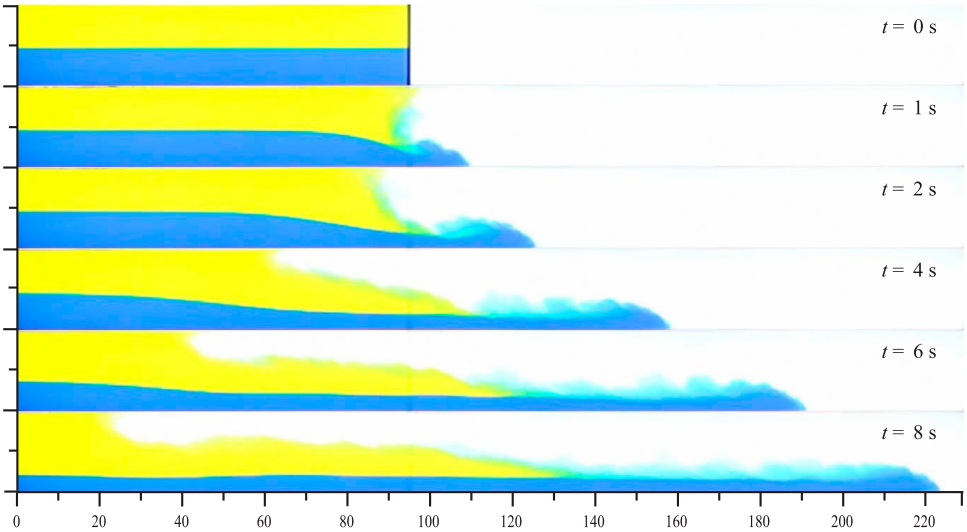

Figure 4 Experiment $08/22/16 - B1$: flow images for the gravity currents produced from a two-layer stratified buoyancy source at $\mathsf{R_B} = 0.2$ and $\mathsf{R_R} = 0.2$. Distances in x and y directions are in units of cm. Time instances are chosen at $t = 0, 1, 2, 4, 6, 8$ s. The slumping phase begins at $t \approx 1.0$ s and the front velocity in the slumping phase is $U_f \approx 16.34\,\mathrm{cm\,s^{-1}}$

fluid collapses out from the lock region, the lower layer forms the front and takes the lead during the propagation of gravity currents in the slumping phase. The upper layer cannot catch up with the lower layer but forms a thin wedge moving on top of the lower layer. In the case $\mathsf{R_R} \ll 1$, there is not as much mixing between the fluids in two layers when compared with the case $\mathsf{R_R} \to 1$, as the images in Fig. 4 show virtually no area in green colour.

Figure 5 shows the front position history of experiment $08/22/16 - B1$. The slumping phase begins at $t \approx 1.0$ s and the stratified gravity currents propagate at a constant speed $U_f \approx 16.34\,\mathrm{cm\,s^{-1}}$, i.e. $\mathsf{F_S} \approx 0.55$. Based on our experimental results, the Froude number in the slumping phase for the lower layer dominated gravity currents produced from a strongly stratified two-layer source is always greater than $\mathsf{F_S} \approx 0.45$, which is the Froude number in the slumping phase for the gravity currents produced from a full-depth homogeneous buoyancy source.

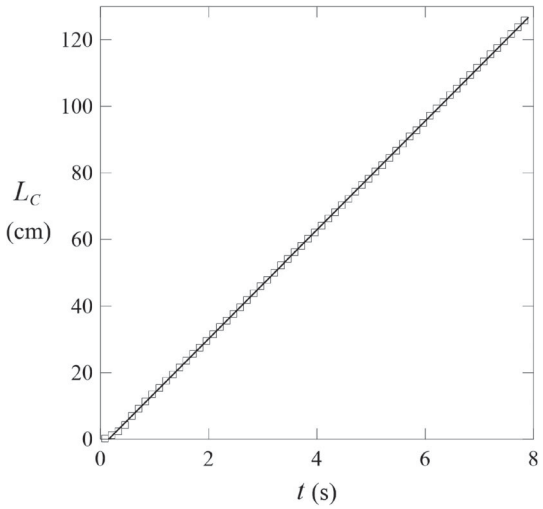

Figure 5 Experiment $08/22/16 - B1$: front position history for the gravity currents produced from a two-layer stratified buoyancy source at $\mathsf{R_B} = 0.2$ and $\mathsf{R_R} = 0.2$. The solid line represents the straight line of best fit to the slumping phase of propagation and the fitting equation is $L_C = 16.34(t + t_0)$, where $t_0 = -0.15$ s

3.2.2 *Weakly stratified two-layer source,* $\mathsf{R_R} \to 1$

For stratified gravity currents dominated by the lower layer and produced from a weakly stratified two-layer source, Fig. 6 shows the flow images of experiment $11/30/16 - C7$ at $\mathsf{R_B} = 0.3$ and $\mathsf{R_R} = 0.8$. As the gravity currents are dominated by the lower layer, the upper layer cannot catch up with the lower layer but moves on top of the lower layer. In the case $\mathsf{R_R} \to 1$, mixing between the fluids in two layers is immediate, as indicated by the green colour areas in the images in Fig. 6.

Figure 7 shows the front position history of experiment $11/30/16 - C7$. The slumping phase begins at $t \approx 1.4$ s and the stratified gravity currents propagate at a constant speed $U_f \approx 13.53\,\mathrm{cm\,s^{-1}}$, i.e. $\mathsf{F_S} \approx 0.464$. For the lower layer dominated gravity currents produced from weakly stratified sources, $\mathsf{R_R} \to 1$, the Froude number in the slumping phase is still greater than but becomes closer to $\mathsf{F_S} \approx 0.45$.

3.3 *Stratified gravity currents dominated by the upper layer,* $0.6 < \mathsf{R_B} < 1.0$

In this section, we present the situation when the gravity currents are dominated by the upper layer, $0.6 < \mathsf{R_B} < 1.0$. In the gravity currents dominated by the upper layer, initially the lower layer takes the lead before the upper layer overrides and outruns the lower layer. Similar to the experiments for lower layer dominated gravity currents, the average density of the two-layer stratified heavy fluid and the density of ambient fluid remain

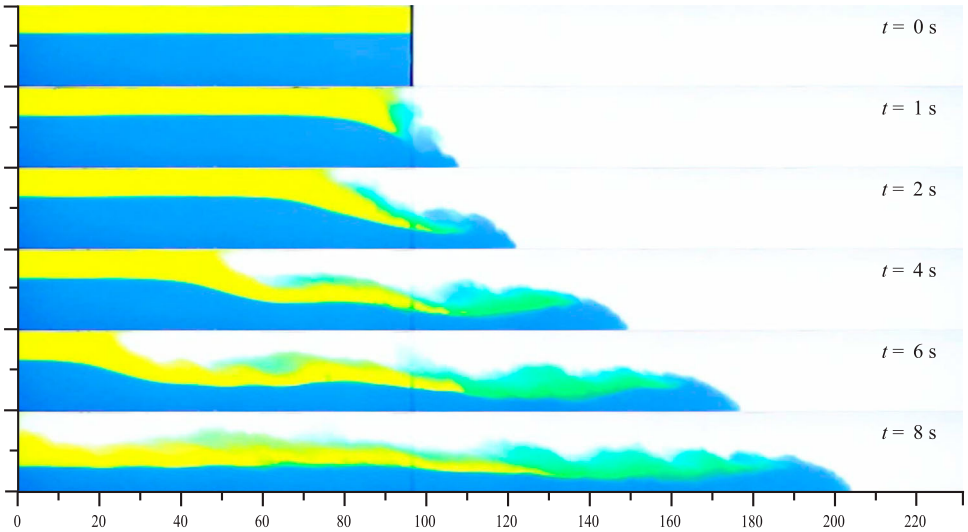

Figure 6 Experiment $11/30/16 - C7$: flow images for the gravity currents produced from a two-layer stratified buoyancy source at $\mathsf{R_B} = 0.3$ and $\mathsf{R_R} = 0.8$. Distances in x and y directions are in units of cm. Time instances are chosen at $t = 0, 1, 2, 4, 6, 8$ s. The slumping phase begins at $t \approx 1.4$ s and the front velocity in the slumping phase is $U_f \approx 13.53\,\mathrm{cm\,s^{-1}}$

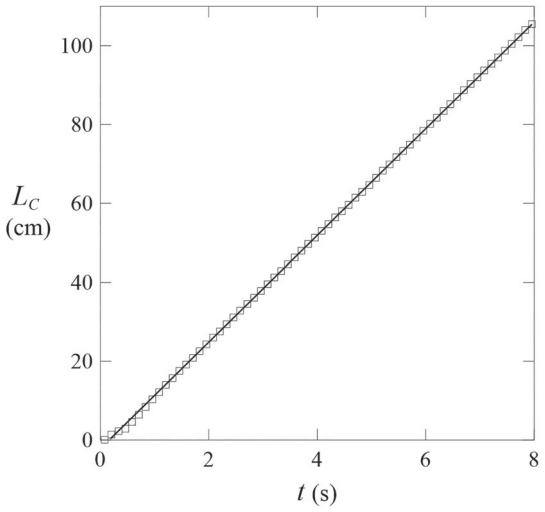

Figure 7 Experiment $11/30/16 - C7$: front position history for the gravity currents produced from a two-layer stratified buoyancy source at $\mathsf{R_B} = 0.3$ and $\mathsf{R_R} = 0.8$. The solid line represents the straight line of best fit to the slumping phase of propagation and the fitting equation is $L_C = 13.53(t + t_0)$, where $t_0 = -0.08$ s

unchanged. Such upper layer dominated gravity currents can also be produced from a strongly stratified source, $\mathsf{R_R} \ll 1$, and from a weakly stratified source, $\mathsf{R_R} \to 1$, and we shall present these flows in order.

3.3.1 *Strongly stratified two-layer source,* $\mathsf{R_R} \ll 1$

For stratified gravity currents dominated by the upper layer and produced from a strongly stratified two-layer source, Fig. 8 shows the flow images of experiment $04/23/17 - G2$ at $\mathsf{R_B} = 0.7$ and $\mathsf{R_R} = 0.2$. After the lock gate is removed, the lower layer takes the lead in the beginning. However, the upper layer overrides and outruns the lower layer afterwards. As shown in Fig. 8 at $t = 2$ s, the upper layer intrudes into the back of the front and, at about $t = 4$ s, the upper layer overrides the lower layer. In the case $\mathsf{R_R} \ll 1$, mixing between the fluids in two layers is not as immediate as in the case $\mathsf{R_R} \to 1$, which is consistent with the observation made for the lower layer dominated gravity currents produced from a strongly stratified source.

Figure 9 shows the front position history of experiment $04/23/17 - G2$. The slumping phase begins at $t \approx 1.8$ s and the stratified gravity currents propagate at a constant speed $U_f \approx 12.31\,\mathrm{cm\,s^{-1}}$, i.e. $\mathsf{F_S} \approx 0.417$. Based on our experimental results, the Froude number in the slumping phase for the upper layer dominated gravity currents produced from a strongly stratified two-layer source is always less than $\mathsf{F_S} \approx 0.45$.

3.3.2 *Weakly stratified two-layer source,* $\mathsf{R_R} \to 1$

For stratified gravity currents dominated by the upper layer and produced from a weakly stratified two-layer source, Fig. 10 shows the flow images of experiment $01/17/17 - H6$ at $\mathsf{R_B} = 0.8$ and $\mathsf{R_R} = 0.7$. As the gravity currents are dominated by the upper layer, the lower layer takes the lead in the beginning but the upper layer overrides and outruns the lower layer afterwards. In the case $\mathsf{R_R} \to 1$, mixing between the fluids in two layers is immediate, as indicated by more green colour areas in the images in Fig. 10.

Figure 11 shows the front position history of experiment $01/17/17 - H6$. The slumping phase begins at $t \approx 2.2$ s and the stratified gravity currents propagate at a constant speed $U_f \approx 13.11\,\mathrm{cm\,s^{-1}}$, i.e. $\mathsf{F_S} \approx 0.447$. It is observed that as the upper layer overruns the lower layer, at $t \approx 6$ s, the front position data slightly deviate from the best fit line but approach towards the best fit line afterwards. For the upper layer dominated gravity currents produced from weakly stratified sources, $\mathsf{R_R} \to 1$, the Froude number in the slumping phase is still less than but becomes closer to $\mathsf{F_S} \approx 0.45$.

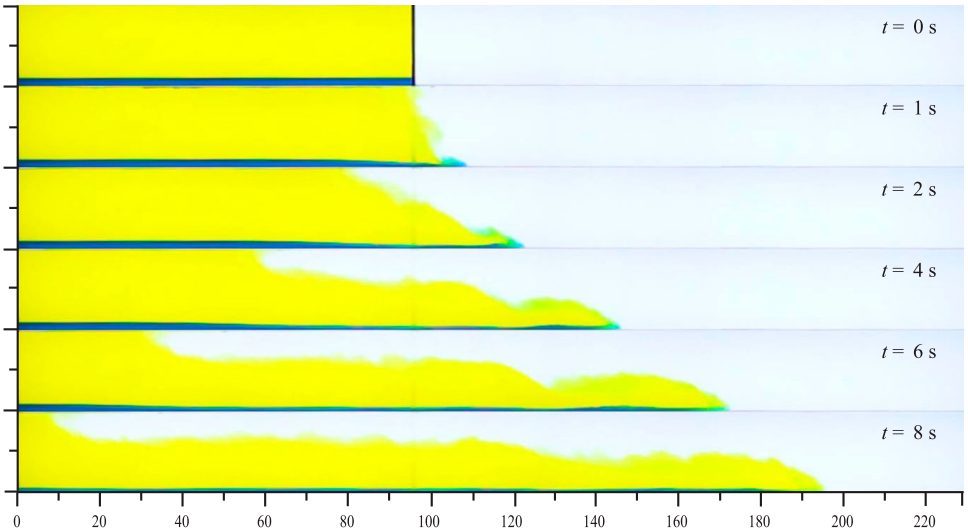

Figure 8 Experiment $04/23/17 - G2$: flow images for the gravity currents produced from a two-layer stratified buoyancy source at $R_B = 0.7$ and $R_R = 0.2$. Distances in x and y directions are in units of cm. Time instances are chosen at $t = 0, 1, 2, 4, 6, 8$ s. The slumping phase begins at $t \approx 1.8$ s and the front velocity in the slumping phase is $U_f \approx 12.31\ \mathrm{cm\,s^{-1}}$

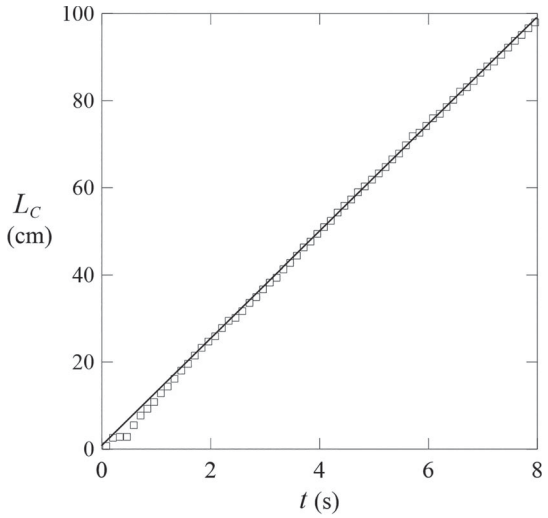

Figure 9 Experiment $04/23/17 - G2$: front position history for the gravity currents produced from a two-layer stratified buoyancy source at $R_B = 0.7$ and $R_R = 0.2$. The solid line represents the straight line of best fit to the slumping phase of propagation and the fitting equation is $L_C = 12.31(t + t_0)$, where $t_0 = 0.09$ s

4 Conclusions

The flow morphology and Froude number in the slumping phase for the two-layer stratified gravity currents are investigated using the experiments. The flow morphology is influenced by the two dimensionless parameters, namely the density difference ratio, R_R, and the buoyancy distribution parameter, R_B. The flow morphology of two-layer stratified gravity currents in the slumping phase can be categorized into two different regimes, namely the gravity currents dominated by the lower layer and those dominated by the upper layer, demarcated by $R_B \approx 0.6$.

Figure 12 shows the flow morphologies of the two-layer stratified gravity currents in three situations, i.e. $R_B < 0.6$, $R_B = 0.6$ and $R_B > 0.6$, while the average density of two-layer heavy fluid and the density of ambient fluid remain unchanged in the experiments and the time instance is chosen at $t = 8$ s for all images in the figure. For the stratified gravity currents dominated by the lower layer, $R_B < 0.6$, the lower layer takes the lead in the slumping phase, as shown in Fig. 12a. In addition, for $R_B < 0.6$, the gravity currents propagate faster as R_R decreases from unity. For the stratified gravity currents with balancing upper layer and lower layer, the two layers propagate approximately at the same speed, as shown in Fig. 12b. For the stratified gravity currents dominated by the upper layer, $R_B > 0.6$, the upper layer overrides and outruns the lower layer. For $R_B > 0.6$, the gravity currents propagate slower as R_R decreases from unity.

Additionally, we attempted to estimate the mixing depth, designated as δ in Fig. 12, and to track its change with the time as a crude measure of mixing rate between the two layers. Based on our experimental results, the flow morphology of lower layer dominated two-layer stratified gravity currents ($R_B \lesssim 0.5$) is qualitatively different from that of upper layer dominated gravity currents flows, depending on the flows dominated by the lower layer ($R_B \gtrsim 0.7$). The time rate of change of mixing depth, represented by $\mathrm{d}\delta/\mathrm{d}t$, is calculated and listed in Table 2. Our results show that, for lower layer dominated two-layer stratified gravity currents, the time rate of change of mixing depth increases as the density difference ratio, R_R, increases. On the other hand, for upper layer dominated gravity currents, the mixing depth is not easily identified, particularly when the stratification between the two layers is strong, i.e. $R_R \ll 1$.

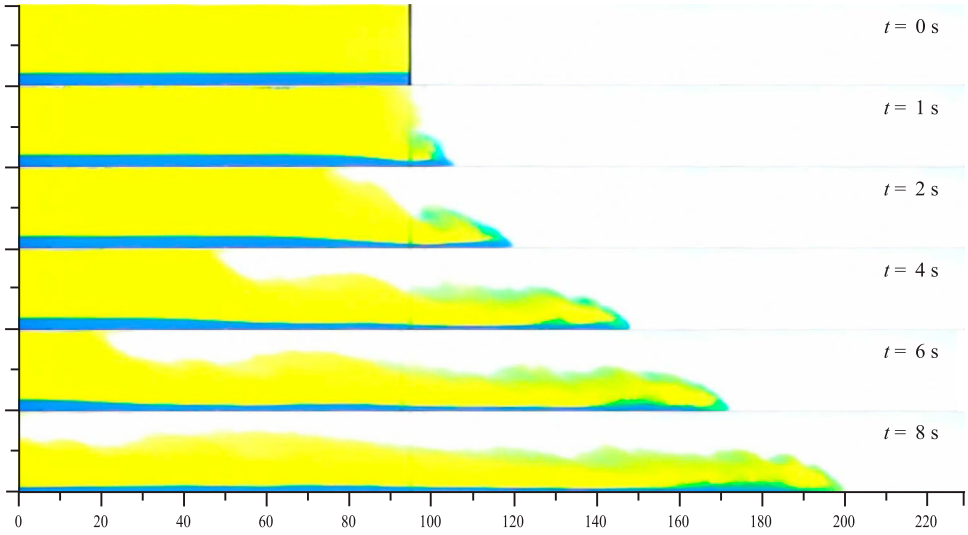

Figure 10 Experiment $01/17/17-H6$: flow images for the gravity currents produced from a two-layer stratified buoyancy source at $\mathsf{R_B} = 0.8$ and $\mathsf{R_R} = 0.7$. Distances in x and y directions are in units of cm. Time instances are chosen at $t = 0, 1, 2, 4, 6, 8$ s. The slumping phase begins at $t \approx 2.2$ s and the front velocity in the slumping phase is $U_f \approx 13.11\ \mathrm{cm\,s^{-1}}$

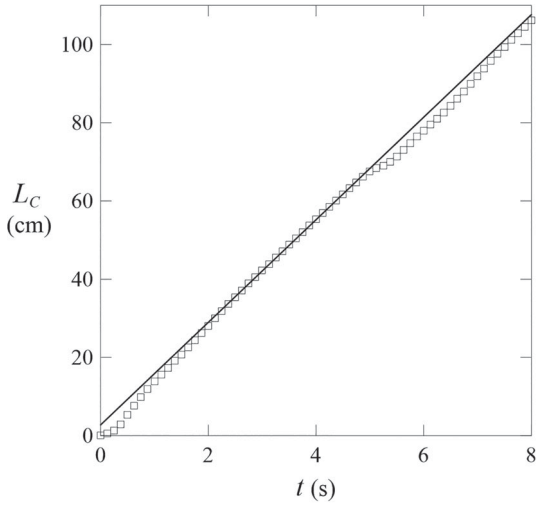

Figure 11 Experiment $01/17/17-H6$: front position history for the gravity currents produced from a two-layer stratified buoyancy source at $\mathsf{R_B} = 0.8$ and $\mathsf{R_R} = 0.7$. The solid line represents the straight line of best fit to the slumping phase of propagation and the fitting equation is $L_C = 13.11(t + t_0)$, where $t_0 = 0.18$ s

Figure 13 shows the Froude number in the slumping phase, defined by Eq. (3), as a function of $\mathsf{R_B}$ and $\mathsf{R_R}$. For the stratified gravity currents dominated by the lower layer, $\mathsf{R_B} < 0.6$, the Froude number in the slumping phase is persistently greater than $\mathsf{F_S} \approx 0.45$. As the two-layer buoyancy source becomes weakly stratified, $\mathsf{R_R} \to 1$, the influence of $\mathsf{R_B}$ diminishes and the Froude number in the slumping phase approaches $\mathsf{F_S} \approx 0.45$. For the stratified gravity currents dominated by the upper layer, $\mathsf{R_B} > 0.6$, the Froude number in the slumping phase is persistently lower than $\mathsf{F_S} \approx 0.45$. Similarly, the influence of $\mathsf{R_B}$ diminishes and the Froude number in the slumping phase approaches $\mathsf{F_S} \approx 0.45$ as $\mathsf{R_R} \to 1$. Additionally, the Froude number in this case is close to the value based on Ungarish (2009) and Hogg et al. (2016), i.e. $\mathsf{F_S} \approx 0.47$. It is interesting to note that, as the buoyancy distribution parameter approaches $\mathsf{R_B} \approx 0.6$, the Froude number in the slumping phase is $\mathsf{F_S} \approx 0.46$ irrespective of the density difference ratio $\mathsf{R_R}$. Such an observation is consistent with our anticipation based on the scaling analysis that, at an intermediate value of $\mathsf{R_B}$, the upper layer and lower layer can propagate forward at the same speed. In other words, for two-layer stratified gravity currents in the slumping phase, it is still possible for the Froude number to be in the proximity of $\mathsf{F_S} \approx 0.45$, provided the buoyancy source is weakly stratified, i.e. $\mathsf{R_R} \to 1$, or provided the buoyancy distribution parameter falls in the proximity of $\mathsf{R_B} \approx 0.6$.

Figure 14 shows the Froude number of two-layer stratified gravity currents as a function of the fractional depth, i.e. $\varphi = h/H$, where h is the thickness of the body of current and H is the total depth of fluid in the channel. Also the Froude number and fractional depth for gravity currents produced from a full-depth homogeneous source are shown for comparison. It is observed that the gravity currents dominated by the upper layer, i.e. $\mathsf{R_B} \geq 0.6$, behave more similarly to the homogeneous case. Gravity currents dominated by the lower layer, i.e. $0.2 \leq \mathsf{R_B} < 0.6$, are more different from those dominated by the upper layer due to the fact that the lower layer takes the lead throughout the slumping phase while the upper layer moves behind as shown in Fig. 12. In this situation the lower layer propagates with smaller fractional depth and larger Froude number. In other words, the flow morphology for two-layer stratified gravity currents dominated by the upper layer is more similar to the homogeneous case, regardless of the disturbances occurring when the upper layer overrides the lower layer.

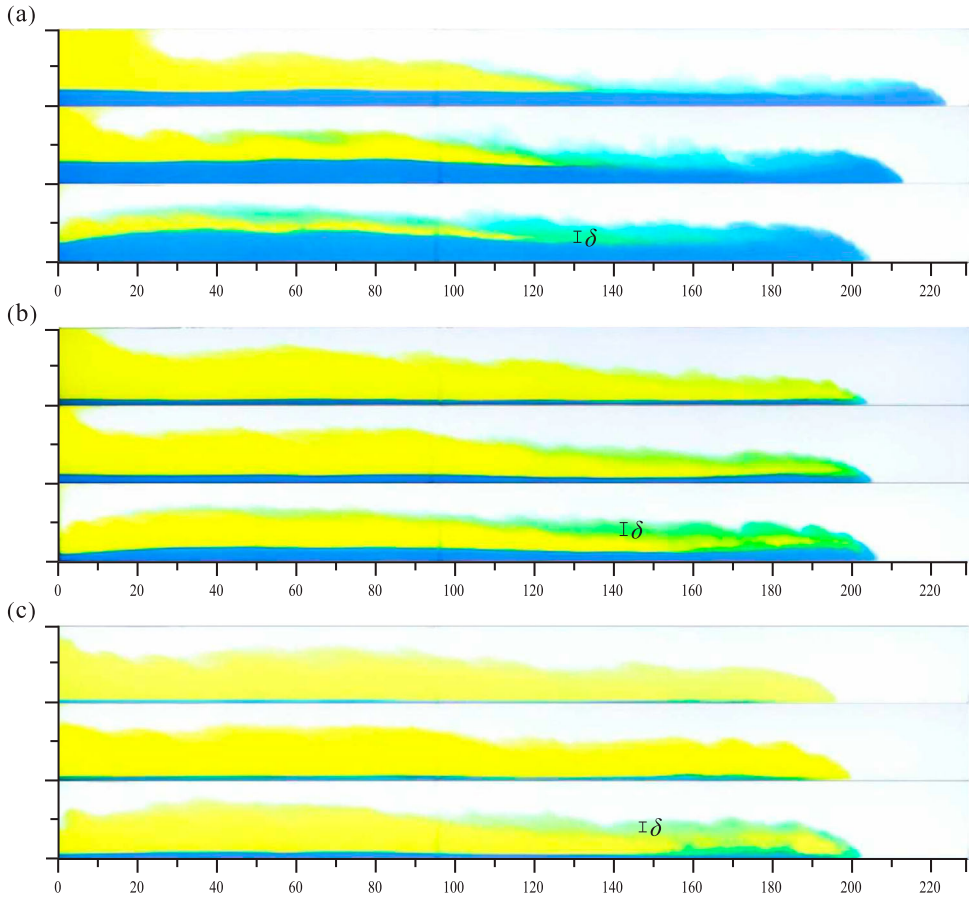

Figure 12 Two-layer stratified gravity currents in the slumping phase in different combinations of R_B and R_R. The time instance is chosen at $t = 8$ s for all images in the figure. The average density in the two-layer buoyancy source is kept constant at $\rho_C = 1.0400\,\mathrm{g\,cm^{-3}}$. Panel (a) shows the stratified gravity currents at $R_B = 0.2$ and $R_R = 0.2$ (top), 0.4 (middle), 0.8 (bottom). Panel (b) shows the stratified gravity currents at $R_B = 0.6$ and $R_R = 0.2$ (top), 0.4 (middle), 0.8 (bottom). Panel (c) shows the stratified gravity currents at $R_B = 0.8$ and $R_R = 0.2$ (top), 0.4 (middle), 0.8 (bottom). The mixing depth is estimated as the thickness of the green area and is designated as δ in the figure

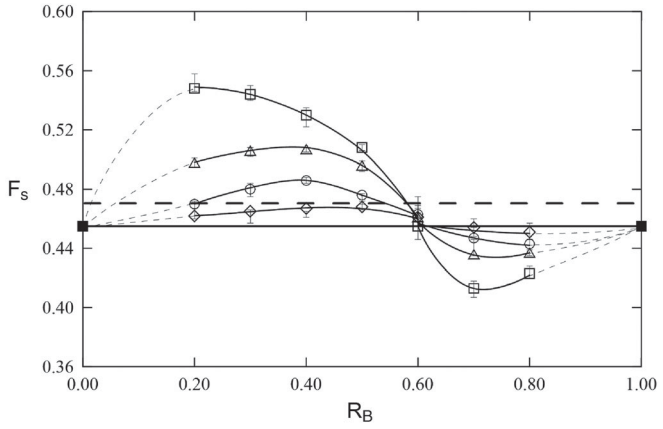

Figure 13 Froude number in the slumping phase, F_S, as a function of the buoyancy distribution parameter, R_B, at four different values of the density difference ratio, $R_R = 0.2$, 0.4, 0.6, 0.8. Symbols: □, $R_R = 0.2$; △, $R_R = 0.4$; °, $R_R = 0.6$; ◇, $R_R = 0.8$. Froude number in the slumping phase produced by a full-depth homogeneous buoyancy source, $F_S = 0.45$, is equivalent to $R_B = 0$ or $R_B = 1$, and $R_R = 1$ and is represented by ■ and the thick solid line. The dashed line represents the value based on Ungarish (2009) and Hogg et al. (2016)

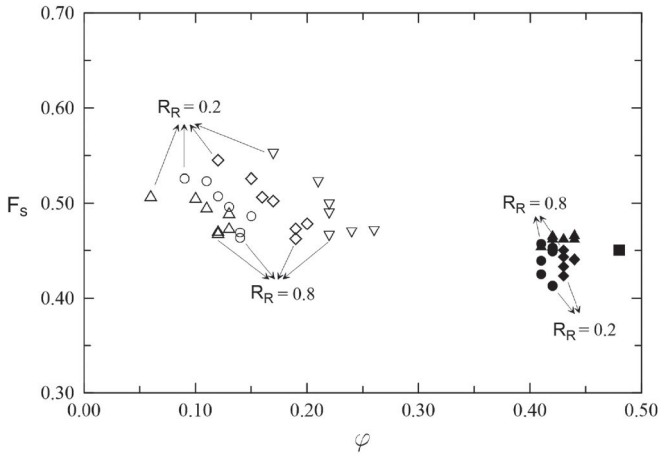

Figure 14 Froude number against fractional depth (φ) for two-layer stratified flows in the slumping phase. Symbols: ▽, $R_B = 0.2$; ◇, $R_B = 0.3$; °, $R_B = 0.4$; △, $R_B = 0.5$; ▲, $R_B = 0.6$; •, $R_B = 0.7$; ♦, $R_B = 0.8$. The case for gravity currents produced from a full-depth homogeneous source is represented by ■

Acknowledgments

The authors would like to thank Mr B.-J. Wen for his help in running the experiments.

Funding

The research was funded by National Taiwan University [grants 106R7739, 106R7830, 107L7830, 107L7734] and by Taiwan Ministry of Science and Technology [grants MOST-104-2628-E-002-012-MY3, MOST-105-2221-E-002-125-MY2, MOST-106-2218-E-197-001].

Notation

B_U = buoyancy in the upper layer ($cm^3\ s^{-2}$)
B_L = buoyancy in the lower layer ($cm^3\ s^{-2}$)
$\mathsf{F_S}$ = Froude number (–)
g = gravitational acceleration ($cm\ s^{-2}$)
g_0' = reduced gravity ($cm\ s^{-2}$)
h_L = thickness of lower layer of two-layer stratified buoyancy source (cm)
h_U = thickness of upper layer of two-layer stratified buoyancy source (cm)
H = total depth of fluid (cm)
L_0 = lock length (cm)
L_C = front position (cm)
$\mathsf{R_B}$ = buoyancy distribution parameter (–)
$\mathsf{R_R}$ = density difference ratio between the upper layer and lower layer (–)
$\mathsf{R_e}$ = Reynolds number (–)
t = time (s)
U = velocity scale ($cm\ s^{-1}$)
U_f = front velocity ($cm\ s^{-1}$)
δ = mixing depth (cm)
ν = kinematic viscosity of fluid ($cm^2\ s^{-1}$)
ρ_0 = density of ambient fluid ($g\ cm^{-3}$)
ρ_C = average density of two-layer heavy fluid ($g\ cm^{-3}$)
ρ_L = fluid density in the lower layer of two-layer stratified buoyancy source ($g\ cm^{-3}$)
ρ_U = fluid density in the upper layer of two-layer stratified buoyancy source ($g\ cm^{-3}$)
φ = fractional depth (–)

References

Adduce, C., Sciortino, G., & Proietti, S. (2012). Gravity currents produced by lock exchanges: Experiments and simulations with a two-layer shallow-water model with entrainment. *Journal of Hydraulic Engineering*, *138*(2), 111–121.

Amen, R., & Maxworthy, T. (1980). The gravitational collapse of a mixed region into a linear stratified fluid. *Journal of Fluid Mechanics*, *96*, 65–80.

Balasubramanian, S., & Zhong, Q. (2018). Entrainment and mixing in lock-exchange gravity currents using simultaneous velocity-density measurements. *Physics of Fluids*, *30*, 056601.

Barr, D. I. H. (1967). Densimetric exchange flows in rectangular channels. *La Houllie Blanche*, *22*, 619–631.

Benjamin, T. B. (1968). Gravity currents and related phenomena. *Journal of Fluid Mechanics*, *31*, 209–248.

Birman, V. K., Meiburg, E., & Ungarish, M. (2007). On gravity currents in stratified ambients. *Physics of Fluids*, *19*, 086602.

Bolster, D., Hang, A., & Linden, P. F. (2008). The front speed of intrusions into a continuously stratified medium. *Journal of Fluid Mechanics*, *594*, 369–377.

Borden, Z., & Meiburg, E. (2013). Circulation based models for Boussinesq gravity currents. *Physics of Fluids*, *25*, 101301.

Cantero, M. I., Lee, J. R., Balachandar, S., & Garcia, M. H. (2007). On the front velocity of gravity currents. *Journal of Fluid Mechanics*, *586*, 1–39.

Cheong, H. B., Kuenen, J. J. P., & Linden, P. F. (2006). The front speed of intrusive gravity currents. *Journal of Fluid Mechanics*, *552*, 1–11.

Dai, A. (2013a). Experiments on gravity currents propagating on different bottom slopes. *Journal of Fluid Mechanics*, *731*, 117–141.

Dai, A. (2013b). Gravity currents propagating on sloping boundaries. *Journal of Hydraulic Engineering*, *139*(6), 593–601.

Dai, A. (2014). Non-Boussinesq gravity currents propagating on different bottom slopes. *Journal of Fluid Mechanics*, *741*, 658–680.

Dai, A. (2017). Experiments on two-layer density stratified inertial gravity currents. *Physical Review Fluids*, *2*, 073802.

Dimotakis, P. E. (2000). The mixing transition in turbulent flows. *Journal of Fluid Mechanics*, *409*, 69–98.

Ellison, T. H., & Turner, J. S. (1959). Turbulent entrainment in stratified flows. *Journal of Fluid Mechanics*, *6*, 423–448.

Flynn, M. R., & Linden, P. F. (2006). Intrusive gravity currents. *Journal of Fluid Mechanics*, *568*, 193–202.

Flynn, M. R., & Sutherland, B. R. (2004). Intrusive gravity currents and internal gravity wave generation in stratified fluid. *Journal of Fluid Mechanics*, *514*, 355–383.

Gladstone, C., Ritchie, L. J., Sparks, R. S. J., & Woods, A. W. (2004). An experimental investigation of density-stratified inertial gravity currents. *Sedimentology*, *51*, 767–789.

Hogg, A. J., Nasr-Azadani, M. M., Ungarish, M., & Meiburg, E. (2016). Sustained gravity currents in a channel. *Journal of Fluid Mechanics*, *798*, 853–888.

Huppert, H. E. (1982). The propagation of two-dimensional and axisymmetric viscous gravity currents over a rigid horizontal boundary surface. *Journal of Fluid Mechanics*, *121*, 43–58.

Johnson, C. G., Hogg, A. J., Huppert, H. E., Sparks, R. S. J., Philips, J. C., A. C. Slim, & Woodhouse, M. J. (2015). Modelling intrusions through quiescent and moving ambients. *Journal of Fluid Mechanics*, *771*, 370–406.

Jones, C. S., Cenedese, C., Chassignet, E. P., Linden, P. F., & Sutherland, B. R. (2014). Gravity current propagation up a valley. *Journal of Fluid Mechanics*, *762*, 417–434.

Keulegan, G. H. (1958). *The motion of saline fronts in still water* (U.S. National Bureau of Standards Report, 5813).

Khodkar, M. A., Allam, K. E., & Meiburg, E. (2018). Intrusions propagating into linearly stratified ambients. *Journal of Fluid Mechanics*, *844*, 956–969.

Khodkar, M. A., Nasr-Azadani, M. M., & Meiburg, E. (2016). Intrusive gravity currents propagating into two-layer stratified ambients: Vorticity modeling. *Physical Review Fluids*, *1*, 044302.

Khodkar, M. A., Nasr-Azadani, M. M., & Meiburg, E. (2018). Gravity currents propagating into two-layer stratified fluids: Vorticity-based models. *Journal of Fluid Mechanics*, *844*, 994–1025.

Koochesfahani, M. M., & Dimotakis, P. E. (1986). Mixing and chemical reactions in a turbulent liquid mixing layer. *Journal of Fluid Mechanics*, *170*, 83–112.

La Rocca, M., Adduce, C., Lombardi, V., Sciortino, G., & Hinkelmann, R. (2012). Developement of a lattice Boltzmann method for two-layered shallow-water flow. *International Journal for Numerical Methods in Fluids*, *70*(8), 1048–1072.

La Rocca, M., Adduce, C., Sciortino, G., & Pinzon, A. B. (2008). Experimental and numerical simulation of three-dimensional gravity currents on smooth and rough bottom. *Physics of Fluids*, *20*(10), 106603.

La Rocca, M., Adduce, C., Sciortino, G., Pinzon, A. B., & Boniforti, M. A. (2012). A two-layer shallow-water model for 3D gravity currents. *Journal of Hydraulic Research*, *50*(2), 208–217.

Lombardi, V., Adduce, C., Sciortino, G., & La Rocca, M. (2015). Gravity currents flowing upslope: Laboratory experiments and shallow-water simulations. *Physics of Fluids*, *27*, 016602.

Marino, B. M., Thomas, L. P., & Linden, P. F. (2005). The front condition for gravity currents. *Journal of Fluid Mechanics*, *536*, 49–78.

Marleau, L. J., Flynn, M. R., & Sutherland, B. R. (2014). Gravity currents propagating up a slope. *Physics of Fluids*, *26*, 046605.

Maxworthy, T., Leilich, J., Simpson, J. E., & Meiburg, E. H. (2002). The propagation of a gravity current into a linearly stratified fluid. *Journal of Fluid Mechanics*, *453*, 371–394.

Nogueira, H. I. S., Adduce, C., Alves, E., & Franca, M. J. (2013a). Analysis of lock-exchange gravity currents over smooth and rough beds. *Journal of Hydraulic Research*, *51*(4), 417–431.

Nogueira, H. I. S., Adduce, C., Alves, E., & Franca, M. J. (2013b). Image analysis technique applied to lock-exchange gravity currents. *Measurement Science and Technology*, *24*, 047001.

Nogueira, H. I. S., Adduce, C., Alves, E., & Franca, M. J. (2014). Dynamics of the head of gravity currents. *Environmental Fluid Mechanics*, *14*(2), 519–540.

Ottolenghi, L., Adduce, C., Inghilesi, R., Roman, F., & Armenio, V. (2016). Mixing in lock-release gravity currents propagating up a slope. *Physics of Fluids*, *28*, 056604.

Samasiri, P., & Woods, A. W. (2015). Mixing in axisymmetric gravity currents. *Journal of Fluid Mechanics*, *782*, R1.

Schooley, A. H., & Hughes, B. A. (1972). An experimental and theoretical study of internal waves generated by the collapse of a two-dimensional mixed region in a density gradient. *Journal of Fluid Mechanics*, *51*, 159–175.

Shin, J. O., Dalziel, S. B., & Linden, P. F. (2004). Gravity currents produced by lock exchange. *Journal of Fluid Mechanics*, *521*, 1–34.

Simpson, J. E. (1997). *Gravity currents: In the environment and the laboratory* (2nd ed.). Cambridge: Cambridge University Press.

Tan, A. W., Nobes, D. S., Fleck, B. A., & Flynn, M. R. (2010). Gravity currents in two-layer stratified media. *Environmental Fluid Mechanics*, *11*, 203–223.

Ungarish, M. (2005). Intrusive gravity currents in a stratified ambient: Shallow-water theory and numerical results. *Journal of Fluid Mechanics*, *535*, 287–323.

Ungarish, M. (2006). On gravity currents in a linearly stratified ambient: A generalization of Benjamin's steady-state propagation results. *Journal of Fluid Mechanics*, *548*, 49–68.

Ungarish, M. (2009). *An introduction to gravity currents and intrusions*. New York: CRC Press.

Ungarish, M., & Hogg, A. J. (2018). Models of internal jumps and the fronts of gravity currents: Unifying two-layer theories and deriving new results. *Journal of Fluid Mechanics*, *846*, 654–685.

Ungarish, M., & Huppert, H. E. (2002). On gravity currents propagating at the base of a stratified ambient. *Journal of Fluid Mechanics*, *458*, 283–301.

Ungarish, M., & Huppert, H. E. (2004). On gravity currents propagating at the base of a stratified ambient: Effects of geometrical constraints and rotation. *Journal of Fluid Mechanics*, *521*, 69–104.

Ungarish, M., & Huppert, H. E. (2006). Energy balances for propagating gravity currents: Homogeneous and stratified ambients. *Journal of Fluid Mechanics*, *565*, 363–380.

White, B. L., & Helfrich, K. R. (2008). Gravity currents and internal waves in a continuously stratified fluid. *Journal of Fluid Mechanics*, *616*, 327–356.

White, B. L., & Helfrich, K. R. (2012). A general description of a gravity current front propagating in a two-layer stratified fluid. *Journal of Fluid Mechanics*, *711*, 545–575.

Wu, J. (1969). Mixed region collapse with internal wave generation in a density-stratified medium. *Journal of Fluid Mechanics*, *35*, 531–544.